Lifetime measurements in ^{96}Rb via fast-timing techniques: Investigating shape coexistence at $A \simeq 100$

E. R. Gamba,[1,2] S. Bottoni,[1,2,*] Ł. W. Iskra,[3,†] C. Zavaglia,[1,2] S. Leoni,[1,2] B. Fornal,[3] N. Cieplicka-Oryńczak,[3] G. Benzoni,[2] G. Colombi,[1,2,4] F. C. L. Crespi,[1,2] A. Esmaylzadeh,[5] M. Jentschel,[4] J. Jolie,[5] V. Karayonchev,[5] Y. H. Kim,[4,‡] L. Knafla,[5] U. Köster,[4] M. Ley,[5] N. Mărginean,[6] R. Mărginean,[6] C. Michelagnoli,[4] M. Polettini,[1,2] C. Porzio,[1,2,§] J-.M. Régis,[5] D. Reygadas,[4] and A. Turturica[6]

[1]*Dipartimento di Fisica, Università degli Studi di Milano, 20133 Milano, Italy*

[2]*INFN Sezione di Milano, 20133, Milano, Italy*

[3]*Institute of Nuclear Physics, PAN, 31-342 Kraków, Poland*

[4]*Institut Laue-Langevin, 38042 Grenoble, France*

[5]*Universität zu Köln, Institut für Kernphysik, 50937 Köln, Germany*

[6]*Horia Hulubei National Institute of Physics and Nuclear Engineering-IFIN HH, Bucharest 077125, Romania*

(Received 29 July 2023; accepted 23 October 2023; published 4 December 2023)

Lifetime measurements of the (3^-), (4^-), and (6^-) intraband states in the neutron-rich, odd-odd ^{96}Rb nucleus were performed at the LOHENGRIN spectrometer of Institut Laue-Langevin, using thermal-neutron-induced fission of ^{235}U and fast-timing techniques with $LaBr_3$: Ce scintillator detectors. The nanosecond isomeric nature of the (3^-) bandhead was established as well as the $\beta_2 = 0.39(3)$ deformation parameter of the band, pointing to a robust deformation in ^{96}Rb. Moreover, a hindered $B(E2)$ value of $3.9^{+19}_{-13} \times 10^{-2}$ W.u. was found for the γ decay of the deformed (4^-) state to the spherical 2^- ground state. A retardation was also found for the $(3^-) \rightarrow 2^-$ transition, possibly due to the shape change and giving strong support to a shape coexistence scenario in this nucleus, at the borders of the island of deformation at $N = 60$. Analogies with the structure of the ^{98}Y isotone are discussed.

DOI: 10.1103/PhysRevC.108.064301

I. INTRODUCTION

In atomic nuclei, the spherical symmetry is firmly established in the vicinity of doubly magic nuclides. However, the interplay between macroscopic (collective) and microscopic (individual nucleons) effects leads to the appearance of deformation and shape coexistence phenomena already in the proximity of shell closures [1,2]. Nowadays, the shape evolution and shape coexistence phenomena are well recognized across the entire nuclear chart and become crucial for understanding various aspects of the nuclear force [3].

In this context, the neutron-rich region around mass $A \approx 100$ is of great importance showing the most striking change of the nuclear shape across isotopic chains [1,2,4,5]. In Rb, Sr, Y, and Zr isotopes, a sudden inversion of spherical and deformed configurations at the ground state was observed at $N = 60$. In the case of the even-$Z = 40$ Zr isotopic chain, calculations based on the Monte Carlo shell model approach [6–8] well reproduce the shape inversion at the ground state, between ^{98}Zr ($N = 58$) and ^{100}Zr ($N = 60$), resulting from a significant modification of nuclear orbitals caused by the monopole terms of the nuclear interaction. This abrupt change of shape can be interpreted in terms of a quantum phase transition (QPT), where the key parameter is the neutron number [6]. A deeper understanding of the QPT process requires the study of nuclei in the transition region near the $N = 60$ boundary.

In the odd-Z Y isotopic chain ($Z = 39$), deformed structures start to be observed in ^{96}Y, i.e., at $N = 57$. Here, a short cascade resembling the beginning of a rotational band is built on the (6^+), 181-ns isomer at 1.655-MeV excitation energy [9,10]. The next odd-odd ^{98}Y ($N = 59$) nucleus shows a rich scenario of shape coexistence [11]: while the ground state and two low-lying isomers are spherical, the two higher located isomers are bandheads of rotational structures. In addition, one of them, based on the $(\pi 5/2^+[422], \nu 3/2^-[541])_{4^-}$ configuration, is fed from a 10^- isomer with a $\pi(g_{9/2})\nu(h_{11/2})$ spherical character. All this makes the ^{98}Y isotope an extraordinary example of shape coexistence phenomena, in which a sequence of decays between states of different shapes is observed: a spherical 10^- state decays towards a 4^- deformed one which, in turn, decays again into a spherical structure at lower excitation energy.

In the odd-Z, ^{96}Rb isotone ($Z = 37$), a similar structure is observed. Here, the spherical (10^-), 2-μs isomer, located at 1.135 MeV, decays into the members of a rotational band built on a deformed $(\pi 3/2^+[431], \nu 3/2^-[541])_{3^-}$ bandhead at 461.6 keV, which subsequently decays into the 2^- ground

*Corresponding author: simone.bottoni@mi.infn.it

†Corresponding author: lukasz.iskra@ifj.edu.pl

‡Present address: Center for Exotic Nuclear Studies, Institute for Basic Science, Daejeon 34126, Republic of Korea.

§Present address: Nuclear Science Division, Lawrence Berkeley National Laboratory, Berkeley, California 94720, USA.

state with a firmly established spherical configuration [12]. A $\pi(f_{5/2})\nu(s_{1/2})$ configuration was proposed for the 2^- ground state [13] according to the measured intrinsic quadrupole moment $Q_0 = 0.86(16)\,eb$, leading to a rather weak deformation parameter $\beta_2 = 0.10(2)$ [14]. For $N \geqslant 60$, ^{97,99}Rb nuclei, the ground state is deformed with observed rotational bands built on it, although with slightly reduced deformation (the deformation parameter is $\beta \approx 0.3$) as compared with other nuclei in this region [15]. On the other hand, in the case of $Z = 36$ Kr isotopes, the low-lying states of ^{96}Kr ($N = 60$) do not show a pronounced collectivity: the energy ratio between the 4_1^+ and 2_1^+ excited states, $R_{4/2} = E(4_1^+)/E(2_1^+) = 2.12$, is in fact consistent with the expectation for a spherical vibrator [16]. Consequently, the Rb isotopic chain can be considered as a low-Z boundary of the region of deformation around $A = 100$. In this context, the ^{96}Rb isotope is at the border of the region of deformed ground states and may serve as a sensitive test of various deformation-driving mechanisms.

In the present work, we performed lifetime measurements by fast-timing techniques in the exotic, neutron-rich ^{96}Rb nucleus. In particular, we focused on the (6^-), (4^-), and (3^-) intraband states at 794.8, 554.5, and 461.6 keV, respectively. The results point to a rather strong deformation of this band, similar to the one observed in Sr, Y, and Zr isotopes with $N \geqslant 60$. Moreover, the nanosecond isomeric nature of the (3^-) bandhead is established, as well as the retardation of the γ transitions connecting the (4^-) and (3^-) states to the spherical 2^- ground state.

The paper is organized as follows. Section II gives a description of the experimental setup. Section III provides details on the experimental analysis and lifetime measurements, while the discussion on shape coexistence and shape evolution is presented in Sec. IV.

II. THE EXPERIMENT

The experiment was carried out at Insititut Laue-Langevin (ILL), where ^{96}Rb nuclei were produced by thermal neutron-induced fission of a ^{235}U target [17] and selected according to their mass-to-charge and energy-to-charge ratios by the LOHENGRIN spectrometer [18]. Fission products were collimated by a refocusing magnet [19] to the focal plane of the spectrometer and detected by an ionization chamber. Their γ decay was measured by one high-energy-resolution HPGe clover detector and four $LaBr_3$: Ce fast scintillators, used for lifetime measurements. These were symmetrically mounted around the ionization chamber and arranged in a standard analog fast-timing setup described in [20] and successfully used in [21]. Considering the time of flight of the fission products of 1.7 μs, only γ-ray cascades emitted from long-lived isomeric states can be measured at the focal plane of the LOHENGRIN spectrometer. In the case of ^{96}Rb, a (10^-) isomeric state at 1135.0 keV with $T_{1/2} = 2$ μs is present, and γ rays feeding lower lying states [12] were observed in this work.

In the experiment, the main source of γ-ray background originates from the radiation emitted by nuclei with a similar mass-to-charge and energy-to-charge ratios, transported to the focal plane along with ^{96}Rb fission fragments, as well as from γ-ray cascades of β^- decays of the implanted ions. In the collected data, ^{96}Sr, ^{96}Y, and ^{96}Zr isobars were all observed. In particular, the β^--decaying 8^+ isomeric state in ^{96}Y, located at 1541 keV, with $T_{1/2} = 9.6$ s, turned out to be the predominant source of γ-ray background. In this experiment, γ-γ coincidence relationships between $LaBr_3$: Ce detectors were used to select the cascades of interest for lifetime measurements. The same gating conditions were used between the crystals of the HPGe Clover detector to monitor possible contaminants with higher energy resolution (see Fig. 1). Given $T_{1/2} = 2$ μs of the (10^-) isomeric state at 1135 keV in

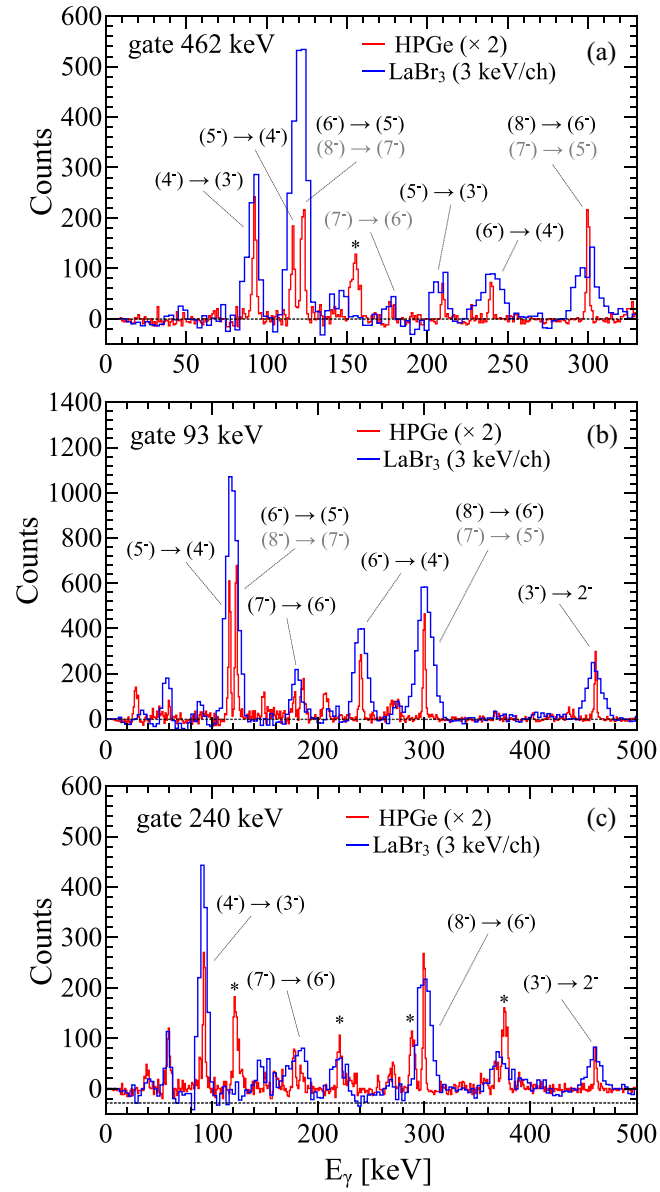

FIG. 1. HPGe (red) and $LaBr_3$: Ce (blue) γ-ray energy spectra gated on the 461.6-keV, $(3^-) \rightarrow 2^-$ (a), 92.8-keV $(4^-) \rightarrow (3^-)$ (b), and 240.3-keV $(6^-) \rightarrow (4^-)$ (c) γ rays in ^{96}Rb. Coincident transitions depopulating the (10^-) isomer are marked in black, with weak lines displayed in gray. The peaks marked by a star come from the Compton scattering of γ rays in the HPGe crystals of the clover detector and enter the spectrum as random coincidences.

^{96}Rb, different time coincidence windows were considered to build γ-γ events, in order to optimize the peak-to-background ratio and the statistics in the $LaBr_3$: Ce spectra. With a trigger imposed on the ionization chamber, a time coincidence window of 5 μs was chosen. The selectivity achieved in the current experiment via γ-γ coincidences is shown in Fig. 1, where the projected spectrum, gated on the 461.6-keV, $(3^-) \rightarrow 2^-$, 92.8-keV $(4^-) \rightarrow (3^-)$, and 240.3-keV $(6^-) \rightarrow (4^-)$ transitions of ^{96}Rb are shown both for HPGe crystals (red) and $LaBr_3$: Ce detectors (blue) in panels (a), (b), and (c), respectively. The entire coincident γ-ray cascades from the 10^- isomer can be seen, except for the 40-keV line depopulating the isomeric state and feeding the (8^-) state. Also, weaker γ-ray branches from the (3^-) and (4^-) states could not be observed due to the limited statistics. In the picture, weak transitions are labeled in gray and they partially overlap with other γ rays. Despite the little statistics collected (few hundreds of counts), given by the exotic nature of ^{96}Rb, clean coincidences were obtained for transitions populating and depopulating the (6^-), (4^-), and (3^-) intraband states and lifetimes could be extracted, as discussed in Sec. III. This was possible thanks to the very low level of the γ-ray background which can be achieved with this setup, as already stressed in Ref. [21]. On the other hand, for the (7^-) and (5^-) states the statistics was not sufficient to firmly measure lifetime values.

III. LIFETIME MEASUREMENTS

Lifetime measurements of intraband states in ^{96}Rb were performed using $LaBr_3$: Ce scintillators and fast-timing techniques [20,22]. A $E_{start}(LaBr_3 : Ce)$-$E_{stop}(LaBr_3 : Ce)$-Δt cube was built to correlate γ-γ coincident energies (E_{start}-E_{stop}), measured in the $LaBr_3$: Ce detectors, with the corresponding time difference Δt, as described in Refs. [21–26]. By applying two-dimensional gates (E_{start}, E_{stop}) and (E_{stop}, E_{start}), being E_{start} and E_{stop} the energies of the γ rays feeding and decaying from the state of interest, two time distributions are obtained, called delayed (D) and antidelayed (AD), respectively. Lifetimes were measured both with the *generalized centroid difference* (GCD) method [20,22] and the *convolution method* [23,24]. In the first case, the ΔC centroid difference between the D and AD time distributions is obtained by measuring their center of gravity from which the lifetimes τ can be determined by

$$2\tau = \Delta C - PRD(E_{feeder}, E_{decay}), \quad (1)$$

where the *prompt response difference* (PRD) correction accounts for time-walk effects of low-energy γ rays [20,22]. This method can be applied to measure lifetimes down to a few ps [21], well below the time resolution of the $LaBr_3$: Ce detectors (of the order of 300 ps). On the other hand, when lifetimes are longer than tens of ps, the D and AD time distributions present an exponential-decaying tail and the *convolution method* can be applied. This consists in fitting the time distributions to the function of a Gaussian component convoluted with an exponential decay, as the one given in Ref. [27]. In general, it is good practice to constrain all the parameters of the convolution function to the experimental data, as indicated in Ref. [24]. In this work, source data were used to determine the width of the Gaussian prompt time distributions, while its centroid position was fixed using the one obtained from the PRD curve for a similar energy combination of start-stop transitions. The integral of the convolution function was constrained on the area of the experimental histograms. In both methods, Compton- and random-background coincident γ rays were accounted for by applying the procedure described in Refs. [28,29] and successfully used in [21,25,26,29,30]. This is aimed at determining the real centroid position of the D and AD time distributions by using Eq. (15) of Ref. [28], without a direct subtraction of background events. The uncertainty on lifetime values is obtained by error propagation of Eq. (15) of Ref. [28], including the error on the PRD correction. The subtraction between time spectra is preferably to be avoided, for the reasons explained in Ref. [28], however, the decision of using a background subtraction procedure, instead of correcting for the centroid position, was taken in some of the cases presented here. This applies to long lifetimes, i.e., ≈1 ns or more, characterized by an extended exponential-decaying tail, which does not allow for a clean identification of the time interval to compute the center of gravity of the time distributions.

A. The (3^-) level at 461.6 keV

The delayed and antidelayed time distributions of the (3^-) level, located at 461.6 keV, were obtained by applying gates on the $(4^-) \rightarrow (3^-)$ and $(3^-) \rightarrow 2^-$ coincident transitions with energy of 92.8 keV and 461.6 keV, feeding and depopulating the level of interest, respectively. The background-subtracted D and AD time distributions are presented in Fig. 2(a) in black and red, respectively. Since the exponential-decaying tails shown by the two time distributions are long compared to the time resolution of the system, the *convolution method* was used to extract lifetimes. The fits performed on the D and AD background-subtracted time distributions are shown in Fig. 2(a) as solid lines and returned the lifetime values of $\tau_D = 3471(1037)$ ps and $\tau_{AD} = 2743(954)$ ps, which are consistent within 1σ. The weighted average between D and AD values gives $\tau_{3^-}^{Conv} = 3077(702)$ ps, which corresponds to $T_{1/2} = 2.13(50) \times 10^3$ ps. We note that the fit of the tail of the time distributions to the function of an exponential decay were also performed, giving consistent results [$T_{1/2} = 1926(595)$ ps]. As the prompt region is avoided when performing a simple exponential decay fit, the choice of the fit range results in larger uncertainties on the lifetime values.

B. The (4^-) level at 554.5 keV in ^{96}Rb

The delayed and antidelayed time distributions of the (4^-) level, located at 554.5 keV, were obtained by applying gates on the $(6)^- \rightarrow (4^-)$ and $(4)^- \rightarrow (3^-)$ coincident transitions with energy of 240.3 keV and 92.8 keV, feeding and depopulating the level of interest, respectively. In this case it was possible to measure the lifetime of the (4^-) level by using both the GCD and the *convolution method* as the two time distributions showed larger statistics and less extended exponential-decaying tails, compared to the (3^-) case. The background-subtracted delayed and antidelayed time

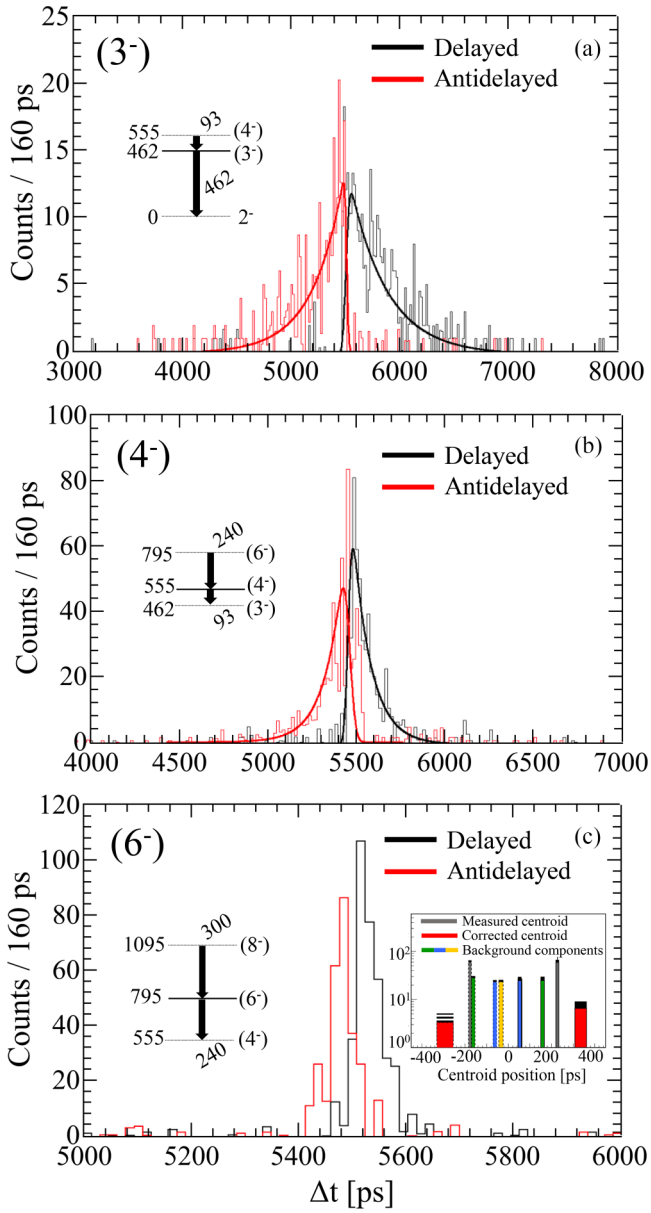

FIG. 2. Delayed (black) and antidelayed (red) time distributions for the (3^-) (a), (4^-) (b), and (6^-) (c) states in ^{96}Rb located at 461.6, 554.5, and 794.8 keV, respectively. The feeding and decaying transitions used to measure the time distributions are shown in the inset. In (a) and (b), the fit results are also shown as solid lines with the same color code. In (c), the centroid positions of the delayed and antidelayed peak and background components are shown in the inset (see text for details). The obtained half-lives are $T_{1/2} = 2.13(50) \times 10^3$ ps, $T_{1/2} = 599(55)$ ps, and $T_{1/2} = 223(32)$ ps for the (3^-), (4^-), and (6^-) states, respectively.

distributions and the fitting curves are presented in Fig. 2(b). The *convolution method* returned lifetime values of $\tau_{\rm D} = 934(155)$ ps and $\tau_{\rm AD} = 889(224)$ ps for the D and AD cases, respectively. The results are consistent within 1σ and the weighted average between the two lifetimes gives $\tau_{4^-}^{\rm Conv} = 919(127)$ ps.

The GDC method was applied by measuring the center of gravity positions of the D and AD time distributions and also centroid position of the background components (see [28] for details). For each background component, gates were applied to the left and to the right of the coincidence peak and the two obtained time distributions were averaged out. For consistency with the previous method, the energy ranges of the gates were the same. Considering the correction PRD$(240.3, 92.8) = -60(6)$ ps, the lifetime was obtained by Eq. (1), giving $\tau_{4^-}^{\rm GCD} = 829(101)$ ps. Given the consistency between the lifetime value obtained from the *convolution method* and the one provided by the GCD method, the weighted average between these measurements is $\tau_{4^-} = 864(79)$ ps, which corresponds to $T_{1/2} = 599(55)$ ps.

C. The (6^-) level at 794.8 keV in ^{96}Rb

The delayed and antidelayed time distributions of the (6^-) level, located at 794.8 keV, were obtained by applying gates on the $(8)^- \rightarrow (6^-)$ and $(6)^- \rightarrow (4^-)$ coincident transitions with energy 300.0 keV and 240.3 keV, feeding and depopulating the level of interest, respectively. In this case, no clear exponential-decaying tails could be observed, hence the lifetime of the (6^-) state was measured with the GCD method only. The D and AD time distributions are presented in Fig. 2(c). The inset shows the position of the center of gravity of the measured centroid (gray) of the D and AD time distributions (solid and dashed lines, respectively) and their background components (yellow, green, and blue), using the graphical representation discussed in Refs. [21,26]. The bar position indicates the centroid value, while its width represents the associated uncertainty. The height of each bar is equal to the number of counts in the corresponding time distributions and the black area on top indicates the uncertainty associated to it. The corrected centroid position is shown in red. The obtained background-corrected centroid difference between the delayed and antidelayed time distributions was $\Delta C = 629(93)$ ps. This, together with a time-walk correction of PRD$(300.0, 240.3) = -14(4)$ ps, yielded a lifetime value of $\tau_{6^-} = 321(46)$ ps, which corresponds to $T_{1/2} = 223(32)$ ps.

IV. DISCUSSION

The lifetimes measured in Sec. III enabled to determine the $B(E2)$ reduced transition probabilities for the $(6^-) \rightarrow (4^-)$ intraband and $(4^-) \rightarrow 2^-$ extraband transitions at 240.3 and 554.5 keV, respectively. Partial lifetime values were obtained from known γ-ray branching ratios and electron conversion coefficients [12,31], when the character of the transition was known. The results are presented in Table I and Fig. 3. The $B(E2)$ value of the $(6^-) \rightarrow (4^-)$ transition is 62^{+16}_{-12} W.u. which points to a significant collectivity of the rotational band, in agreement with the description given in Ref. [12]. This result was obtained assuming the conversion electron coefficient of a pure $M1$ transition for the 135.5-keV γ-ray branch, as it connects the 6^- state to the 5^- state. This is done consistently with the 5^- to 4^- transition which has a firmly established $M1$ character. The β_2 deformation parameter was obtained from the measured $B(E2)$ value via the equation

$$\beta_2 = \frac{4\pi\sqrt{B(E2; I_i \rightarrow I_f)}}{3R^2 Z |\langle J_i K 20 | J_f K \rangle|}, \qquad (2)$$

TABLE I. Energies, spins, parities, and decay properties of the (6^-), (4^-), and (3^-) states in ^{96}Rb, studied in this work. Level and γ-ray energies are taken from [12]. The $T_{1/2}$ half-lives and the $B(E/M\lambda)$ values measured in this work are reported. For the 461.6-keV γ ray, the extreme cases of a pure $M1$ and $E2$ γ transition are given. The γ-ray intensities and multipolarities were taken from Ref. [12] while electron conversion coefficients α are taken from Ref. [31]. The β_2 value here deduced from the $(6^-) \rightarrow (4^-)$ decay is also reported.

E_i [keV]	I_i	$T_{1/2}$ [ps]	E_f [keV]	I_f	E_γ [keV]	α	BRγ [%]	$E/M\lambda$	$B(E/M\lambda)$ [W.u.]	$\lvert\beta_2\rvert$
794.8	(6^-)	223(32)	554.5	(4^-)	240.3	$3.95(6)\times 10^{-2}$	50.9(26)	[$E2$]	62^{+16}_{-12}	0.39(3)
554.5	(4^-)	599(55)	0.0	2^-	554.5	$2.52(4)\times 10^{-3}$	5.7(11)	[$E2$]	$3.9^{+19}_{-13}\times 10^{-2}$	
461.6	(3^-)	$2.13(50)\times 10^3$	0.0	2^-	461.6	$2.52(4)\times 10^{-3}$ ($M1$)[a] $4.38(7)\times 10^{-3}$ ($E2$)[b]	85.3(23)	[$M1+E2$]	$9.0^{+32}_{-20}\times 10^{-5}$ (M1)[a] $4.1^{+15}_{-10}\times 10^{-1}$ (E2)[b]	

[a]Assuming pure $M1$ character.
[b]Assuming pure $E2$ character.

where $R = 1.2A^{1/3}$ and the $B(E2)$ value is in $e^2\text{fm}^4$. In the Clebsch-Gordan coefficient of Eq. (2), $K = 3$ was considered [12]. The result is $\beta_2 = 0.39(3)$, which is consistent with the lower limit $\beta_2 \geqslant 0.28$ [12] obtained by comparing the computed and experimental $(g_K - g_R)/Q_0$ values, where g_K is the intrinsic gyromagnetic factor and $g_R = Z/A = 0.39$ is the collective gyromagnetic factor. In the same work, an upper limit was also obtained by assuming a g_R value of $0.75 \times Z/A$, as in Ref. [32], leading to $\beta_2 = 0.39$. The β_2 value measured in this work lies right at the upper edge of this deformation window. Turning now to the measured $B(E2)$ value for the $(4)^- \rightarrow 2^-$ transition, the result obtained in this work is $B(E2) = 3.9^{+19}_{-13} \times 10^{-2}$ W.u., which is well below 1 W.u., indicating a strong hindrance of this $E2$ decay. In this case, the only relevant conversion coefficient is the one of the 92.8-keV, $M1$ transition which is properly included in the branch calculation [$\alpha = 0.178(3)$] [31]. For the other transitions of higher energies, the conversion electron correction does not affect the final γ branches, regardless of the character of the transitions. Such a hindrance is possibly due to a shape change between deformed and spherical $\pi(f_{5/2})\nu(s_{1/2})$ configurations. The retardation of the $(4)^- \rightarrow 2^-$ transition is in agreement with a shape-coexistence scenario in which the $(4)^-$ long lived state has the features of a shape-isomer-like structure, similarly to what is observed in the ^{64,66}Ni cases [33,34]. Moreover, the isomeric nature of the 3^- state established in this work is in agreement with its bandhead character, as anticipated in [12]. In this case, the 461.6-keV transition feeding the 2^- ground state has a $M1 + E2$ character but the mixing ratio is not known. Although a pure $E2$ character is unlikely, the two extreme cases of a pure $M1$ and $E2$ transition were considered to extract upper limits on the reduced transition probabilities. Also in this case, the electron conversion coefficients do not have any substantial impact on the γ branch of the 461.6-keV transition of interest. The results are reported in Table I and give $B(M1) = 9.0^{+32}_{-20} \times 10^{-5}$ W.u. and $B(E2) = 4.1^{+15}_{-10} \times 10^{-1}$ W.u., which point to a hindrance of the 461.6-keV γ ray, giving further support to the shape change scenario proposed on the basis of the measured properties of the (4^-) state discussed above. The above results are consistent with theory prediction from Hartree-Fock-Bogoliubov calculations, based on the D1S Gogny effective nucleon-nucleon interaction, according to which two minima in the potential energy surface (PES) of ^{96}Rb are expected [35]. In particular, the prolate minimum lies at $\beta_2 \approx 0.4$, in agreement with the deformation parameter of the rotational band here obtained.

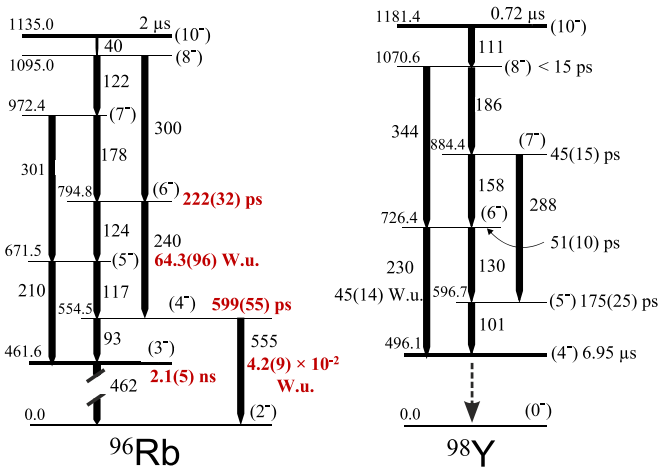

FIG. 3. Comparison between the partial level schemes of ^{96}Rb as measured in this work (left) and ^{98}Y (right) [10,11]. The half-lives and the $B(E2)$ values in ^{96}Rb here obtained are displayed in red.

The structure of ^{96}Rb can be compared to the one of the neighboring ^{98}Y odd-odd nucleus [10,11]. Striking similarities between these two isotones can be recognized by inspecting the partial level schemes presented in Fig. 3. A rotational band fed by a 10^- isomeric state, located slightly above 1100 keV, is observed in both cases. In ^{98}Y, a $\pi(g_{9/2})\nu(h_{11/2})$ spherical configuration was proposed for the 10^- isomer [11], and spherical-like structures above it were identified. Moreover, the ^{98}Y, 10^- isomer is found to decay to deformed structures, originating from the same $\pi g_{9/2}$ and $\nu h_{11/2}$ orbitals via $E2$ transitions. This type of decay is rather exceptional, where the same unique parity states are present in both spherical and deformed configurations, and the analogies between these structures of ^{96}Rb and ^{98}Y points now to a similar scenario in ^{96}Rb, as originally suggested in Ref. [12]. Moreover, the β_2 value of 0.39(3) found in this work for ^{96}Rb is the same as $\beta_2 = 0.40(14)$ of the rotational band in ^{98}Y [9], indicating a robustness of deformation close to the $N = 60$ boundary. The similar structure of the deformed rotational bands in the ^{96}Rb and ^{98}Y isotones can be also seen

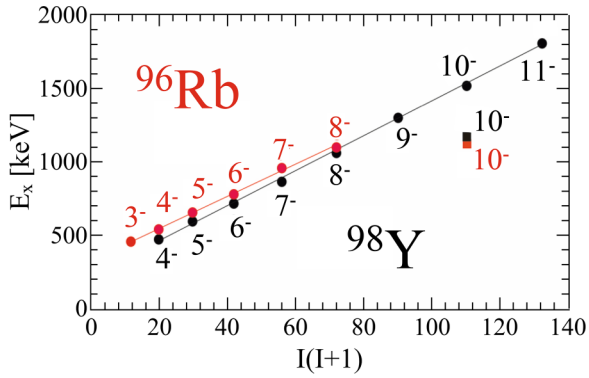

FIG. 4. Excitation energy as a function of $I(I+1)$ for rotational bands built on the (3^-) and (4^-) states in ^{96}Rb (red) and ^{98}Y (black), respectively.

in Fig. 4, where the excitation energy of the states, plotted as a function of $I(I+1)$, indicates the same moment of inertia of 45 $\hbar^2$MeV^{-1}. The bandheads of the rotational bands in ^{96}Rb and ^{98}Y are the (3^-) and (4^-) isomeric states located at 461.6 and 496 keV excitation energy, respectively, with a decay strongly hindered in both cases. In ^{98}Y, the main branch (89.5%) of the 6.95-μs, (4^-) state is the $M1+E2$, 121-keV transition with 0.05 W.u. for the $E2$ component [11]. An even larger degree of retardation is found for the pure $E2$, 325-keV transition, which represents the 2.5% of the (4^-) isomeric decay, with $B(E2) = 2.7 \times 10^{-5}$ W.u. Also for the remaining $E1$, 50-keV branch, the 2×10^{-8} W.u. value is 2–3 orders of magnitude lower than typical $B(E1)$ rates in this mass region. For the corresponding (3^-) bandhead in ^{96}Rb, the main 461.6-keV γ decay feeds the 2^- ground state with a branch of ≈86% [12] and the reduced probability of the $E2$ component of this transition, found in the present work, is lower than $4.1^{+15}_{-10} \times 10^{-1}$ W.u., which is in line with a significant hindrance of the decay (see Table I).

V. CONCLUSIONS

In summary, the lifetimes of the (6^-), (4^-), and (3^-) intraband states in ^{96}Rb were measured at the LOHENGRIN spectrometer of Institut Laue-Langevin using neutron-induced fission of ^{235}U and fast-timing techniques. The ns-isomeric character of the (3^-) bandhead was established as well as the large deformation of the rotational band built on it, with $\beta_2 = 0.39(3)$. The present deformation is very similar to the one reported for the rotational band built on the (4^-) state in the neighboring ^{98}Y isotone, while it is significantly larger than the $\beta \approx 0.3$ value suggested for the $N \geqslant 60$, ^{97,99}Rb nuclei [15]. Finally, a strong hindrance of the γ decays from the (4^-) and (3^-) intraband states to the 2^- spherical ground state were found, possibly ascribed to a shape change. The quantification of the degree of deformation of the rotational band and the retardation of the extraband γ decays found in this work confirm the shape-coexistence scenario in ^{96}Rb, at the low-Z cornerstone of the $A \approx 100$ deformation region.

ACKNOWLEDGMENTS

This work was supported in part by the Italian Istituto Nazionale di Fisica Nucleare, the Polish National Science Centre, Poland, under research Project No. 2020/39/D/ST2/03510, the Polish National Agency for Academic Exchange (NAWA) within the Bekker programme under Grant No. PPN/BEK/2020/1/00431/U/00001, the Institute for Basic Science (IBS-R031-D1), the German DFG under Grant No. JO391/18-1, and the Romanian Ministry of Research, Innovation and Digitization Nucleu Project No. PN 23 21 01 02.

[1] K. Heyde and J. L. Wood, Rev. Mod. Phys. **83**, 1467 (2011).
[2] P. E. Garrett, M. Zielińska, and E. Clément, Prog. Part. Nucl. Phys. **124**, 103931 (2022).
[3] T. Otsuka and Y. Tsunoda, J. Phys. G: Nucl. Part. Phys. **43**, 024009 (2016).
[4] S. Leoni, C. Michelagnoli, and J. N. Wilson, Riv. Nuovo Cim. **45**, 461 (2022).
[5] E. Cheifetz, R. C. Jared, S. G. Thompson, and J. B. Wilhelmy, Phys. Rev. Lett. **25**, 38 (1970).
[6] T. Togashi, Y. Tsunoda, T. Otsuka, and N. Shimizu, Phys. Rev. Lett. **117**, 172502 (2016).
[7] C. Kremer, S. Aslanidou, S. Bassauer, M. Hilcker, A. Krugmann, P. von Neumann-Cosel, T. Otsuka, N. Pietralla, V. Y. Ponomarev, N. Shimizu, M. Singer, G. Steinhilber, T. Togashi, Y. Tsunoda, V. Werner, and M. Zweidinger, Phys. Rev. Lett. **117**, 172503 (2016).
[8] L. W. Iskra, R. Broda, R. Janssens, M. Carpenter, B. Fornal, T. Lauritsen, T. Otsuka, T. Togashi, Y. Tsunoda, W. Walters, and S. Zhu, Phys. Lett. B **788**, 396 (2019).
[9] L. W. Iskra, B. Fornal, S. Leoni, G. Bocchi, A. Petrovici, C. Porzio, A. Blanc, G. D. France, M. Jentschel, U. Köster, P. Mutti, J.-M. Régis, G. Simpson, T. Soldner, C. A. Ur, W. Urban, D. Bazzacco, G. Benzoni, S. Bottoni, A. Bruce, N. Cieplicka-Oryńczak, F. C. L. Crespi, L. M. Fraile, W. Korten, T. Kröll, S. Lalkovski, N. Márginean, C. Michelagnoli, B. Melon, D. Mengoni, B. Million, A. Nannini, D. Napoli, Z. Podolyák, P. H. Regan, and B. Szpak, Europhys. Lett. **117**, 12001 (2017).
[10] L. W. Iskra, S. Leoni, B. Fornal, C. Michelagnoli, F. Kandzia, N. Mărginean, M. Barani, S. Bottoni, N. Cieplicka-Oryńczak, G. Colombi, C. Costache, F. C. L. Crespi, J. Dudouet, M. Jentschel, Y. H. Kim, U. Köster, R. Lica, R. Mărginean, C. Mihai, R. E. Mihai, C. R. Nita, S. Pascu, C. Porzio, D. Reygadas, E. Ruiz-Martinez, and A. Turturica, Phys. Rev. C **102**, 054324 (2020).
[11] W. Urban, M. Czerwiński, J. Kurpeta, T. Rząca-Urban, J. Wiśniewski, T. Materna, L. W. Iskra, A. G. Smith, I. Ahmad, A. Blanc, H. Faust, U. Köster, M. Jentschel, P. Mutti, T. Soldner, G. S. Simpson, J. A. Pinston, G. de France, C. A. Ur, V.-V. Elomaa, T. Eronen, J. Hakala, A. Jokinen, A. Kankainen, I. D. Moore, J. Rissanen, A. Saastamoinen, J. Szerypo, C. Weber, and J. Äystö, Phys. Rev. C **96**, 044333 (2017).
[12] J. A. Pinston, J. Genevey, R. Orlandi, A. Scherillo, G. S. Simpson, I. Tsekhanovich, W. Urban, H. Faust, and N. Warr, Phys. Rev. C **71**, 064327 (2005).

[13] J. Genevey, F. Ibrahim, J. A. Pinston, H. Faust, T. Friedrichs, M. Gross, and S. Oberstedt, Phys. Rev. C **59**, 82 (1999).
[14] C. Thibault, F. Touchard, S. Büttgenbach, R. Klapisch, M. de Saint Simon, H. T. Duong, P. Jacquinot, P. Juncar, S. Liberman, P. Pillet, J. Pinard, J. L. Vialle, A. Pesnelle, and G. Huber, Phys. Rev. C **23**, 2720 (1981).
[15] C. Sotty, M. Zielińska, G. Georgiev, D. L. Balabanski, A. E. Stuchbery, A. Blazhev, N. Bree, R. Chevrier, S. Das Gupta, J. M. Daugas, T. Davinson, H. De Witte, J. Diriken, L. P. Gaffney, K. Geibel, K. Hadyńska-Klęk, F. G. Kondev, J. Konki, T. Kröll, P. Morel, P. Napiorkowski, J. Pakarinen, P. Reiter, M. Scheck, M. Seidlitz, B. Siebeck, G. Simpson, H. Törnqvist, N. Warr, and F. Wenander, Phys. Rev. Lett. **115**, 172501 (2015).
[16] J. Dudouet, A. Lemasson, G. Duchêne, M. Rejmund, E. Clément, C. Michelagnoli, F. Didierjean, A. Korichi, G. Maquart, O. Stezowski, C. Lizarazo, R. M. Pérez-Vidal, C. Andreoiu, G. de Angelis, A. Astier, C. Delafosse, I. Deloncle, Z. Dombradi, G. de France, A. Gadea, A. Gottardo, B. Jacquot, P. Jones, T. Konstantinopoulos, I. Kuti, F. Le Blanc, S. M. Lenzi, G. Li, R. Lozeva, B. Million, D. R. Napoli, A. Navin, C. M. Petrache, N. Pietralla, D. Ralet, M. Ramdhane, N. Redon, C. Schmitt, D. Sohler, D. Verney, D. Barrientos, B. Birkenbach, I. Burrows, L. Charles, J. Collado, D. M. Cullen, P. Désesquelles, C. Domingo Pardo, V. González, L. Harkness-Brennan, H. Hess, D. S. Judson, M. Karolak, W. Korten, M. Labiche, J. Ljungvall, R. Menegazzo, D. Mengoni, A. Pullia, F. Recchia, P. Reiter, M. D. Salsac, E. Sanchis, C. Theisen, J. J. Valiente-Dobón, and M. Zielińska, Phys. Rev. Lett. **118**, 162501 (2017).
[17] https://dx.doi.org/10.5291/ill-data.3-01-688.
[18] P. Armbruster, M. Asghar, J. Bocquet, R. Decker, H. Ewald, J. Greif, E. Moll, B. Pfeiffer, H. Schrader, F. Schussler, G. Siegert, and H. Wollnik, Nucl. Instrum. Methods **139**, 213 (1976).
[19] G. Fioni, H. Faust, M. Gross, M. Hesse, P. Armbruster, F. Gönnenwein, and G. Münzenberg, Nucl. Instrum. Methods Phys. Res. A **332**, 175 (1993).
[20] J.-M. Régis, A. Esmaylzadeh, J. Jolie, V. Karayonchev, L. Knafla, U. Köster, Y. Kim, and E. Strub, Nucl. Instrum. Methods Phys. Res. A **955**, 163258 (2020).
[21] S. Bottoni, E. R. Gamba, G. De Gregorio, A. Gargano, S. Leoni, B. Fornal, N. Brancadori, G. Ciconali, F. C. L. Crespi, N. Cieplicka-Oryńczak, L. W. Iskra, G. Colombi, Y. H. Kim, U. Köster, C. Michelagnoli, F. Dunkel, A. Esmaylzadeh, L. Gerhard, J. Jolie, L. Knafla, M. Ley, J.-M. Régis, K. Schomaker, and M. Sferrazza, Phys. Rev. C **107**, 014322 (2023).
[22] J.-M. Régis, H. Mach, G. Simpson, J. Jolie, G. Pascovici, N. Saed-Samii, N. Warr, A. Bruce, J. Degenkolb, L. Fraile, C. Fransen, D. Ghita, S. Kisyov, U. Koester, A. Korgul, S. Lalkovski, N. Mărginean, P. Mutti, B. Olaizola, Z. Podolyák *et al.*, Nucl. Instrum. Methods Phys. Res. A **726**, 191 (2013).
[23] H. Mach, M. Moszyński, R. Gill, F. Wohn, J. Winger, J. C. Hill, G. Molnár, and K. Sistemich, Phys. Lett. B **230**, 21 (1989).
[24] N. Mărginean, D. L. Balabanski, D. Bucurescu, S. Lalkovski, L. Atanasova, G. Căta-Danil, I. Căta-Danil, J. M. Daugas, D. Deleanu, P. Detistov, G. Deyanova, D. Filipescu, G. Georgiev, D. Ghiţă, K. A. Gladnishki, R. Lozeva, T. Glodariu, M. Ivaşcu, S. Kisyov, C. Mihai, R. Mărginean, A. Negret, S. Pascu, D. Radulov, T. Sava, L. Stroe, G. Suliman, and N. V. Zamfir, Eur. Phys. J. A **46**, 329 (2010).
[25] E. R. Gamba, A. M. Bruce, S. Lalkovski, M. Rudigier, S. Bottoni, M. P. Carpenter, S. Zhu, J. T. Anderson, A. D. Ayangeakaa, T. A. Berry, I. Burrows, M. C. Gallardo, R. J. Carroll, P. Copp, D. M. Cullen, T. Daniel, G. F. Martínez, J. P. Greene, L. A. Gurgi *et al.*, Phys. Rev. C **100**, 044309 (2019).
[26] M. Rudigier, P. Walker, R. Canavan, Z. Podolyák, P. Regan, P.-A. Söderström, M. Lebois, J. Wilson, N. Jovancevic, A. Blazhev, J. Benito, S. Bottoni, M. Brunet, N. Cieplicka-Oryńczak, S. Courtin, D. Doherty, L. Fraile, K. Hadyńska-Klek, M. Heine, L. Iskra *et al.*, Phys. Lett. B **801**, 135140 (2020).
[27] K. Lan and J. W. Jorgenson, J. Chromatogr., A **915**, 1 (2001).
[28] E. Gamba, A. Bruce, and M. Rudigier, Nucl. Instrum. Methods Phys. Res. A **928**, 93 (2019).
[29] V. Werner, N. Cooper, J.-M. Régis, M. Rudigier, E. Williams, J. Jolie, R. B. Cakirli, R. F. Casten, T. Ahn, V. Anagnostatou, Z. Berant, M. Bonett-Matiz, M. Elvers, A. Heinz, G. Ilie, D. Radeck, D. Savran, and M. K. Smith, Phys. Rev. C **93**, 034323 (2016).
[30] R. L. Canavan, M. Rudigier, P. H. Regan, M. Lebois, J. N. Wilson, N. Jovancevic, P.-A. Söderström, S. M. Collins, D. Thisse, J. Benito, S. Bottoni, M. Brunet, N. Cieplicka-Oryńczak, S. Courtin, D. T. Doherty, L. M. Fraile, K. Hadyńska-Klek, G. Häfner, M. Heine, L. W. Iskra *et al.*, Phys. Rev. C **101**, 024313 (2020).
[31] T. Kibédi, T. Burrows, M. Trzhaskovskaya, P. Davidson, and C. Nestor, Nucl. Instrum. Methods Phys. Res. A **589**, 202 (2008).
[32] H. Mach, F. K. Wohn, M. Moszyn'ski, R. L. Gill, and R. F. Casten, Phys. Rev. C **41**, 1141 (1990).
[33] S. Leoni, B. Fornal, N. Mărginean, M. Sferrazza, Y. Tsunoda, T. Otsuka, G. Bocchi, F. C. L. Crespi, A. Bracco, S. Aydin, M. Boromiza, D. Bucurescu, N. Cieplicka-Oryńczak, C. Costache, S. Călinescu, N. Florea, D. G. Ghiţă, T. Glodariu, A. Ionescu, L. W. Iskra, M. Krzysiek, R. Mărginean, C. Mihai, R. E. Mihai, A. Mitu, A. Negreţ, C. R. Niţă, A. Olăcel, A. Oprea, S. Pascu, P. Petkov, C. Petrone, G. Porzio, A. Şerban, C. Sotty, L. Stan, I. Ştiru, L. Stroe, R. Şuvăilă, S. Toma, A. Turturică, S. Ujeniuc, and C. A. Ur, Phys. Rev. Lett. **118**, 162502 (2017).
[34] N. Mărginean, D. Little, Y. Tsunoda, S. Leoni, R. V. F. Janssens, B. Fornal, T. Otsuka, C. Michelagnoli, L. Stan, F. C. L. Crespi, C. Costache, R. Lica, M. Sferrazza, A. Turturica, A. D. Ayangeakaa, K. Auranen, M. Barani, P. C. Bender, S. Bottoni, M. Boromiza, A. Bracco, S. Călinescu, C. M. Campbell, M. P. Carpenter, P. Chowdhury, M. Ciemała, N. Cieplicka-Oryńczak, D. Cline, C. Clisu, H. L. Crawford, I. E. Dinescu, J. Dudouet, D. Filipescu, N. Florea, A. M. Forney, S. Fracassetti, A. Gade, I. Gheorghe, A. B. Hayes, I. Harca, J. Henderson, A. Ionescu, L. W. Iskra, M. Jentschel, F. Kandzia, Y. H. Kim, F. G. Kondev, G. Korschinek, U. Köster, Krishichayan, M. Krzysiek, T. Lauritsen, J. Li, R. Mărginean, E. A. Maugeri, C. Mihai, R. E. Mihai, A. Mitu, P. Mutti, A. Negret, C. R. Niţă, A. Olăcel, A. Oprea, S. Pascu, C. Petrone, C. Porzio, D. Rhodes, D. Seweryniak, D. Schumann, C. Sotty, S. M. Stolze, R. Şuvăilă, S. Toma, S. Ujeniuc, W. B. Walters, C. Y. Wu, J. Wu, S. Zhu, and S. Ziliani, Phys. Rev. Lett. **125**, 102502 (2020).
[35] J. Berger, M. Girod, and D. Gogny, Comput. Phys. Commun. **63**, 365 (1991).